CHEMISTRY OF MATERIALS
Article

Chem. Mater. **2010,** *22,* 261–271 261
DOI:10.1021/cm903038w

From Ultrafine Thiolate-Capped Copper Nanoclusters toward Copper Sulfide Nanodiscs: A Thermally Activated Evolution Route

Derrick Mott,[†] Jun Yin,[†] Mark Engelhard,[‡] Rameshwori Loukrakpam,[†] Paul Chang,[†] George Miller,[§] In-Tae Bae,[⊥] Narayan Chandra Das,[⊥] Chongmin Wang,[‡] Jin Luo,[†] and Chuan-Jian Zhong*,[†]

[†]*Department of Chemistry, State University of New York at Binghamton, Binghamton, New York 13902,* [‡]*Environmental and Molecular Sciences Laboratory, Pacific Northwest National Laboratory, Richland, Washington 99352,* [§]*AFRL/RHPG, Brooks City-Base, San Antonio, Texas, and* [⊥]*S*^{3}*IP Analytical and Diagnostics Laboratory, State University of New York at Binghamton, Binghamton, New York 13902*

Received September 30, 2009. Revised Manuscript Received November 3, 2009

This report shows that the size, shape, and composition of presynthesized copper nanoparticles can be nanoengineered through exploiting concurrent interparticle aggregative growth and interfacial carbon−sulfur cleavage in a thermally activated evolution route. This is demonstrated by thermally activated processing of ultrafine copper nanoclusters encapsulated with thiolate monolayer ($Cu_n(SR)_m$) toward semiconducting copper sulfide (Cu_2S) nanodiscs with controllable sizes and shapes. Under controlled temperatures (120−150 °C), the ultrafine $Cu_n(SR)_m$ nanoclusters, with a size of ∼0.5 nm evidenced by TEM, SAXS-WAXS, DCP-AES, and MALDI-TOF measurements, were shown to evolve into thiolate-capped Cu_2S nanodiscs via thermally activated coalescence and copper-catalyzed interfacial C−S cleavage reactivities. The Cu_2S nanodiscs, as confirmed by XPS and HRTEM analyses, exhibited controllable and monodispersed sizes depending on the thermal processing parameters, ranging from 5 to 35 nm in the disk dimension and 3−6 nm in the thickness dimension. These nanodiscs are stable and display remarkable 1D/2D ordering upon self-assembly. This process is not a simple digestive ripening of smaller particles because it involves an aggregative nucleation and growth process distinctively different from traditional ripening and a reactive carbon−sulfur bond cleavage controlled by the catalytic effect of copper under the specified temperatures. The coupling of the thermally activated coalescence and C−S bond cleavage to convert the ultrafine Cu nanoclusters toward the formation of Cu_2S nanodiscs is highly effective for tuning nanoscale size, shape, and composition, and could find applications in nanoengineering a variety of semiconducting nanocrystals for applications in nanostructured electronic, sensing, and photochemical devices.

Introduction

We wish to report a thermally activated evolution strategy for the fabrication of copper(I) sulfide (Cu_2S) nanoparticles from ultrafine copper nanoclusters as precursors. Cu_2S is interesting because of its semiconducting properties with a bulk bandgap of 1.2 eV.[1] Although the use of Cu_2S thin films in combination with CdS has been known to be useful in Cu_2S/CdS solar cells,[1] the limitation in bandgap tuning and stability has been a long-standing problem. The recent demonstration of the ability in the control of size, shape, and doping-related stability using nanocrystal-based approaches has led to increasing interests in this class of materials. The semiconductor properties of Cu_2S make it ideal for applications in cold cathodes, nanoscale switches, as well as many varieties of solar cells including dye-sensitized, inorganic nanoparticle, and nanocrystal-polymer solar cells.[1,2] Recently, there have been a few excellent reports on the synthesis of Cu_2S nanocrystals.[1,3−6] Alivisatos and co-workers reported the synthesis of Cu_2S nanocrystals (5 nm) using injection reaction of copper(II) acetylacetonate and ammonium diethyldithiocarbamate in a mixed solvent of dodecanethiol and oleic acid.[1] Such nanocrystals have also been demonstrated as an active light-absorbing component in combination with CdS nanorods to make a solution-processed solar cell with 1.6% power conversion efficiency on both conventional glass substrates and flexible plastic substrates. The synthesis of copper sulfide nanostructures such as nanoparticles, nanodiscs,

*To whom correspondence should be addressed. E-mail: cjzhong@binghamton.edu.

(1) Wu, Y.; Wadia, C.; Ma, W.; Sadtler, B.; Alivisatos, A. P. *Nano Lett*. **2008**, *8*, 2551.
(2) Zhuang, Z.; Peng, Q.; Zhang, B.; Li, Y. *J. Am. Chem. Soc*. **2008**, *130*, 10482.
(3) Larsen, T. H.; Sigman, M. B.; Ghezelbash, A.; Doty, R. C.; Korgel, B. A. J. Am. Chem. Soc.,**2003**, *125*, 5638.
(4) Matsumoto, T.; Fujii, H.; Ueda, T.; Kamai, M.; Nogi, K. *Meas. Sci. Technol*. **2005**, *16*, 432.
(5) Karabacak, T.; DeLuca, J. S.; Wang, P.-I.; Ten Eyck, G. A.; Ye, D.; Wang, G.-C.; Lu, T.-M. *J. Appl. Phys*. **2006**, *99*, 064394.
(6) Sigman, M. B.; Ghezelbash, A.; Hanrath, T.; Saunders, A. E.; Lee, F.; Korgel, B. A. *J. Am. Chem. Soc*. **2003**, *125*, 16050.

Published on Web 11/30/2009

nanorods, nanoflowers, and nanowires, as well as their assembly into large arrays[2,3,6−8] have attracted recent interests. Korgel and co-workers demonstrated the synthesis of copper sulfide nanodiscs by thermolysis of alkanethiols and copper(II) nitrate in a solventless reaction in which copper(II) was complexed with octanoate and dodecanethiolate ligands before thermolysis.[3,6] Li and co-workers demonstrated the synthesis of copper sulfide nanocrystals using a two-phase method in an autoclave reactor in which the reaction between dodecanethiol in toluene solution and Cu(II) in aqueous solution produced Cu_2S nanocrystals at the water−toluene interface.[2] These prior methods have demonstrated excellent capabilities in synthesizing Cu_2S nanocrystals using Cu(II) compounds as precursors.

In view of the nanoscale tuning of size and shape from nanoparticles,[9] the viability of creating Cu_2S nanocrystals using copper nanoparticles as precursors would be intriguing from both fundamental and practical perspectives. This idea stems from the increasing number of reports demonstrating the capability of synthesizing copper nanoparticles using various methods, including organic encapsulation in aqueous phase, [10,11] or using mixed-reverse micelles as a template to control the size and shape of copper nanoparticles.[12] Different shapes such as spheres, cubes, or wires were also obtained by using a wide variety of different capping agents in the reduction of $Cu(OH)_2$ with hydrazine.[13] The synthesis of copper nanoparticles in organic phase,[14−16] and by thermal decomposition,[17,18] have also been accomplished. In addition, a wide range of techniques exist for the synthesis of copper nanomaterials including physical vapor deposition,[19,20] chemical vapor deposition,[21] γ-irradiation,[22] UV-light irradiation,[23] and sonochemical methods.[24] Despite the wide range of approaches employed toward monometallic copper nanoparticles, many techniques show either limited monodispersity in size or shape or are susceptible to oxidation.[14,25] The synthesis of copper nanoparticles of different sizes was recently demonstrated in our laboratory by a combination of chemical reduction of Cu(II) to form small-sized particles and a subsequent thermally activated coalescence to form larger-sized particles.[9] The size control of this method took advantage of both the encapsulation of the particles with oleic acid and oleylamine[17] and the interparticle coalescence as a result of melting-point decrease for small-sized copper particles.[26] The melting temperature is theoretically shown to drop dramatically as size decreases to nanometer or subnanometer.[9] The surface melting temperature could be even lower under mild heating conditions in a solution, as supported by both theoretical[4,5] and experimental studies.[27−29] For example, a copper nanoparticle with a diameter below 4 nm is expected to exhibit a melting point below 200 °C.[9,12,30] Conceptually, the thermal processing induces an evolution of the precursor nanoparticles to form larger-sized or shaped nanoparticles via thermally activated desorption of capping molecules, coalescence of nanocrystal seeds, and re-encapsulation of the larger-sized particles. However, under this condition, the size evolution does not impact the oxidation state of the metal, and therefore does not change the composition of the resulting nanoparticles.

In this report, we demonstrate that the size, shape, and composition of the ultrafine (~0.5 nm) copper nanoclusters encapsulated with thiolates[26] can be thermally processed toward copper sulfide nanodiscs with controllable sizes and shapes. This approach explores the viability of a thermally activated coalescence of ~0.5 nm sized copper nanoparticles and a concurrent Cu−thiolate reactivity toward the formation of copper sulfide nanocrystals with well-defined nanodisc shapes. This concept advances our previous demonstration of thermal processing of gold, copper, and alloy nanoparticles[26] by exploring the concurrent reactivity of the copper and capping thiolate molecules in the thermally activated coalescence process. Scheme 1 illustrates such a thermally activated

(7) Tian, C.; Kang, Z.; Wang, E.; Gao, L.; Wang, C.; Xu, L.; Hu, C. *Mater. Lett.* **2005**, *59*, 1156.
(8) (a) Chen, C.; Zhu, C.; Hao, L.; Hu, Y.; Chen, Z. *Chem. Lett.* **2004**, *33*, 898. (b) Li, S.; Wang, H. Z.; Xu, W. W.; Si, H. L.; Tao, X. J.; Lou, S.; Du, Z.; Li, L. S. *J. Colloid Interface Sci.* **2009**, *330*, 483. (c) Peng, M.; Ma, L. L.; Zhang, Y. G.; Tan, M.; Wang, J. B.; Yu, Y. *Mater. Res. Bull.* **2009**, *44*, 1834.
(9) Mott, D.; Galkowski, J.; Wang, L.; Luo, J.; Zhong, C. J. *Langmuir* **2007**, *23*, 5740.
(10) Kim, Y. H.; Kang, Y. S.; Lee, W. J.; Jo, B. G.; Jeong, J. H. *Mol. Cryst. Liq. Cryst.* **2006**, *445*, 231.
(11) Kobayashi, Y.; Sakuraba, T. *Colloids Surf., A* **2008**, *317*, 756.
(12) Lisiecki, I.; Sack-Kongehl, H.; Weiss, K.; Urban, J.; Pileni, M.-P. *Langmuir* **2000**, *16*, 8802.
(13) (a) Wu, S.; Chen, D. *J. Colloid Interface Sci.* **2004**, *273*, 165. (b) Zhou, G.; Lu, M.; Yang, Z. *Langmuir* **2006**, *22*, 5900. (c) Chang, Y.; Lye, M. L.; Zeng, H. C. *Langmuir* **2005**, *21*, 3746. (d) Huang, H.; Yan, F.; Kek, Y.; Chew, C.; Xu, G.; Ji, W.; Oh, P.; Tang, S. *Langmuir* **1997**, *13*, 172.
(14) Chen, S.; Sommers, J. M. *J. Phys. Chem. B* **2001**, *105*, 8816.
(15) Yang, J.; Chen, S. *Acta Chim. Sin.* **2007**, *65*, 2243.
(16) Pastoriza-Santos, A.; Sánchez-Iglesias, B.; Rodríguez-González; Liz-Marzán, L. M. *Small* **2009**, *5*, 440.
(17) (a) Sun, S.; Murray, C. B.; Weller, D.; Folks, L.; Moser, A. *Science* **2000**, *278*, 1989. (b) Fievet, F.; Lagier, J. P.; Figlarz, M. *MRS Bull.* **1989**, *14*, 29.
(18) Cha, S. I.; Mo, C. B.; Kim, K. T.; Jeong, Y. J.; Hong, S. H. *J. Mater. Res.* **2006**, *21*, 2371.
(19) Wang, J.; Huang, H.; Kesapragada, S. V.; Gall, D. *Nano. Lett.* **2005**, *5*, 2505.
(20) Vitulli, G.; Bernini, M.; Bertozzi, S.; Pitzalis, E.; Salvadori, P.; Coluccia, S.; Martra, G. *Chem. Mater.* **2002**, *14*, 1183.
(21) (a) Wang, T.; Yang, W.; Wu, L.; Chen, C.; Chu, C. *Nanotechnology* **2006**, *17*, 719. (b) Kim, C.; Gu, W.; Briceno, M.; Robertson, I. M.; Choi, H.; Kim, K. *Adv. Mater.* **2008**, *20*, 1859. (c) Choi, H.; Park, S. H. *J. Am. Chem. Soc.* **2004**, *126*, 6248.
(22) Henglein, A. *J. Phys. Chem. B* **2000**, *104*, 1206.
(23) Kapoor, S.; Palit, D. K.; Mukherjee, T. *Chem. Phys. Lett.* **2002**, *355*, 383.
(24) Vijaya Kumar, R.; Mastai, Y.; Diamanta, Y.; Gedanken, A. *J. Mater. Chem.* **2001**, *11*, 1209.
(25) (a) Dhas, N. A.; Raj, C. P.; Gedanken, A. *Chem. Mater.* **1998**, *10*, 1446. (b) Zhu1, H.; Zhang, C.; Yin, Y. *Nanotechnology.* **2005**, *16*, 3079.
(26) (a) Maye, M. M.; Zheng, W. X.; Leibowitz, F. L.; Ly, N. K.; Zhong, C. J. *Langmuir* **2000**, *16*, 490. (b) Schadt, M. J.; Cheung, W.; Luo, J.; Zhong, C. J. *Chem. Mater.* **2006**, *18*, 5147.
(27) Ressler, T.; Kniep, B. L.; Kasatkin, I.; Schlögl, R. *Angew. Chem.* **2005**, *44*, 4704.
(28) (a) Vukojevic, S.; Trapp, O.; Grunwaldt, J.; Kiener, C.; Schth, F. *Angew. Chem., Int. Ed.* **2005**, *44*, 7978. (b) Barrabes, N.; Just, J.; Dafinov, A.; Medina, F.; Fierro, J. L. G.; Sueiras, J. E.; Salagre, P.; Cesteros, Y. *Appl. Catal., B* **2006**, *62*, 77.
(29) Dick, K.; Dhanasekaran, T.; Zhang, Z.; Meisel, D. *J. Am. Chem. Soc.* **2002**, *124*, 2312.
(30) Buffat, Ph.; Borel, J. P. *Phys. Rev. A* **1976**, *13*, 2287.

Scheme 1. Illustration of the Thermally Activated Evolution Route from Ultrafine Thiolate-Capped Cu Nanoclusters toward Thiolate-Capped Cu_2S Nanocrystals: Thermally-Activated Interfacial C−S Cleavage and Interparticle Nanocluster Coalescence

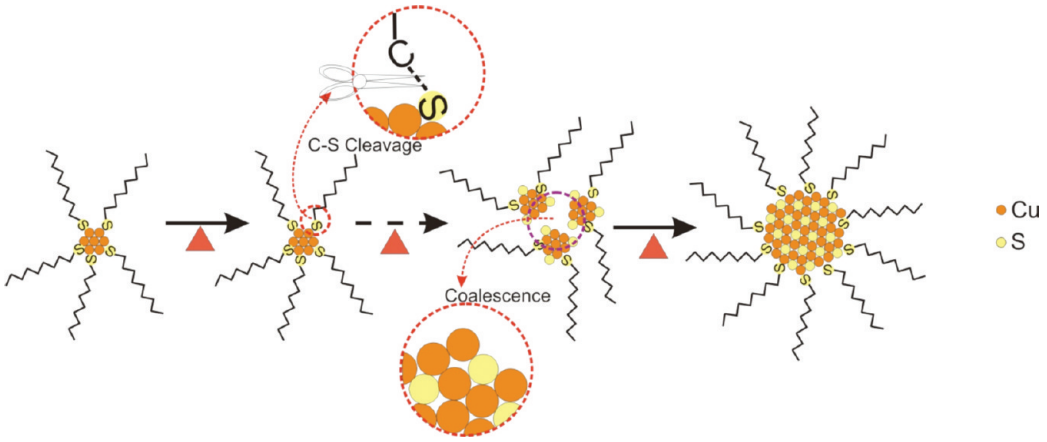

coalescence of the $Cu_n(SR)_m$ nanocluster seeds accompanied by an interfacial C−S bond cleavage toward the formation of Cu_2S nanocrystals.

The interparticle coalescence takes advantage of the particle size effect on the melting temperature of nanoparticles,[26] whereas the interfacial C−S cleavage is catalyzed by copper at the elevated temperature.[3,6] This report shows that this combination operates for thiolate-capped Cu nanoparticles, in contrast to copper nanoparticles capped with oleic acid and oleyl amine,[9] which to the best of our knowledge represents the first example in exploring the "coalescence−cleavage" strategy for the size, shape, and composition control of copper sulfide nanocrystals.

Experimental Section

Chemicals. Copper(II) chloride dihydrate ($CuCl_2 \cdot 2H_2O$, 99%) and copper(II) acetylacetonate ($Cu(acac)_2$, 98%) were obtained from Alfa Aesar. 1-Decanethiol (DT, 96%), 1,2-hexadecanediol (90%), octyl ether (99%), oleyl amine (OAM, 70%), and potassium bromide (99%) were obtained from Sigma Aldrich. Tetra-*n*-octylammonium bromide (TOABr, 98%) and oleic acid (OAC, 99%) were obtained from Alfa Aesar. Sodium borohydride (99%), hexane, and other common solvents used were obtained from Aldrich. Water was purified with a Millipore Direct-Q system (18.2 MΩ·cm).

Synthesis and Thermal Processing. DT-Cu nanoparticles. The synthesis of DT-capped copper nanoparticles was achieved by modification of a previously reported method,[4] which is similar to the two-phase synthesis of gold nanoparticles.[14] In the modified synthesis, $CuCl_2$ was dissolved in water (40 mM) in the presence of 430 mM potassium bromide to convert Cu^{2+} to $CuBr_4^{2-}$. This solution was then mixed with a solution of TOABr in toluene (40 mL of toluene, 1 g of TOABr) under vigorous stirring to induce a phase transfer of the $CuBr_4^{2-}$ from the aqueous phase to the organic phase.[3,31] After being stirred for 45 min, the aqueous solution was removed, leaving a deep maroon-colored organic phase. The copper toluene solution was stirred under an argon purge to eliminate all oxygen from the system. After the solution was purged for 30 min, 1.0 mL of decanethiol was added, causing the solution color to change from maroon to clear. Next, 10 mL of a solution of sodium borohydride in water (1 M) was added dropwise to the solution. The solution became a deep cloudy orange, indicating the formation of copper nanoparticles. The solution was stirred under argon for 2 h. The solution was then subjected to rotary evaporation to eliminate excess toluene. To further increase the conversion of Cu^{2+} to $CuBr_4^{2-}$ for the phase transfer, we also used an increased amount of Br^-. For example, $CuCl_2$ was dissolved in water (565 mM) in the presence of 4.3 M KBr, and this solution was then mixed with a solution of TOABr in toluene (80 mL of toluene, 180 mM TOABr) under vigorous stirring to induce a phase transfer of $CuBr_4^{2-}$ from the aqueous phase to the organic phase. After 45 min of vigorous stirring, the aqueous solution was removed. The copper toluene solution was stirred under an argon purge to eliminate all oxygen from the system. After 30 min of purging, 2.0 mL of decanethiol was added to the toluene solution under argon, causing the solution to change color from deep maroon to a clear yellow-green. Ten milliliters of a 1 M solution of $NaBH_4$ in water was added dropwise to the solution. The solution was stirred under argon for 2 h before rotary evaporation to eliminate excess toluene, resulting in a thick viscous orange suspension.

The suspension of the Cu nanoparticles was used as precursors (or seeds) for the subsequent thermal processing. After rotary evaporation (~20x concentration factor) the particles displayed a deeper orange/amber color, indicative of the higher concentration of particles. The suspension (~4 mL) was contained in a glass vial that was kept in an oven with controlled temperature for a controlled period of time. The thermal processing included a set of predetermined temperatures ranging from 127 to 142 °C.[5] After removal from the oven, the suspension was cooled to room temperature, which displayed a dark brown/orange color. The particles were further cleaned using ethanol. The nanoparticles were soluble in hexane and stable in air for many weeks.

OAM/OAC-capped Cu nanoparticles were also synthesized by modification of previous methods reported for the synthesis of bimetallic[26,32] and trimetallic nanoparticles.[3] Briefly, $Cu(acac)_2$ was added to octyl ether to create a 20 mM solution of Cu(II). 1,2-Hexadecanediol (a reducing agent) was added to the solution (60 mM). The solution was heated under argon to a temperature of 105 °C with stirring. Oleic acid and oleyl amine capping agents were added to the solution to create 20 mM

(31) Dong, T-. Y.; Wu, H-. H.; Lin, M-. C. *Langmuir* **2006**, *22*, 6754.

(32) Wang, L.; Shi, X.; Kariuki, N. N.; Schadt, M.; Wang, G. R.; Rendeng, Q.; Choi, J.; Luo, J.; Lu, S.; Zhong, C. J. *J. Am. Chem. Soc.* **2007**, *129*, 2161.

solutions of each. The solution was heated to higher temperatures, which was varied from 150 to 210 °C. After reaction for 30 min, the solution was cooled to room temperature. By adding ethanol to precipitate the particles, the supernatant was removed and the nanoparticles were washed. The nanoparticles were dried under nitrogen.

Instrumentation and Measurements. An array of techniques, including small-angle X-ray scattering (SAXS) and wide-angle X-ray scattering (WAXS), transmission electron microscopy (TEM), high-resolution TEM (HRTEM), X-ray diffraction (XRD), X-ray photoelectron spectroscopy (XPS), Auger electron spectroscopy (AES), and matrix-assisted laser desorption/ionization time-of-flight (MALDI-TOF) mass spectrometry, were used to characterize the size, shape, and composition of the nanoparticles.

TEM analysis was performed on an Hitachi H-7000 electron microscope (100 kV). For samples that required a higher resolution, an FEI Tecnai T12 Spirit Twin TEM/SEM electron microscope (120 kV) was utilized. Copper nanoparticle samples were suspended in hexane solution and were drop cast onto a carbon-coated copper grid followed by solvent evaporation in air at room temperature. HRTEM was also carried out using a JEOL JEM 2010F with an acceleration voltage of 200 kV and a routine point-to-point resolution of 0.194 nm.

XRD data was collected on a Philips X'Pert diffractometer using Cu Kα radiation (λ = 1.5418 Å). The diffraction (Bragg) angles 2θ were scanned at a step of 0.025°. Each data point was measured for at least 20 s and several scans were taken of the sample.

XPS and AES measurements were collected using a Physical Electronics Quantum 2000 Scanning ESCA Microprobe. This system uses a focused monochromatic Al Kα X-ray (1486.7 eV) source and a spherical section analyzer. The instrument has a 16 element multichannel detector. The X-ray beam used was 100 W with 100 mm diameter and was rastered over a 1.3 mm by 0.2 mm rectangle on the sample. The X-ray beam is incident normal to the sample and the photoelectron detector was at 45° off-normal. Wide scan data was collected using a pass energy of 117.4 eV. For the $Ag3d_{5/2}$ line, these conditions produce fwhm of better than 1.6 eV. High energy resolution photoemission spectra were collected using a pass energy of 46.95 eV. For the $Ag3d_{5/2}$ line, these conditions produced fwhm of better than 0.77 eV. The binding energy (BE) scale is calibrated using the $Cu2p_{3/2}$ feature at 932.62 ± 0.05 eV and Au4f at 83.96 ± 0.05 eV for known standards. The sample experienced variable degrees of charging. The vacuum chamber pressure during analysis was $< 1.3 \times 10^{-6}$ Pa. Samples were dropped onto a molybdenum substrate and were allowed to dry. The C1s peak was used as an internal standard (284.9 eV) for the calibration of the binding energy.

SAXS/WAXS patterns of copper nanoparticle suspensions were recorded at room temperature with Cu Kα radiation from a 1.2 kW rotating anode X-ray generator (007 HF, Rigaku Denki Co. Ltd., Japan), and both two-dimensional multiwire detector and image plate were used for low and high scattering angle respectively. The sample−detector distance of 1.5 (SAXS) and 34.8 mm (WAXS) allowed a "q range" from 0.006 to 0.12 $Å^{-1}$ and 0.1 to 4 $Å^{-1}$ ($q = 4\pi/\lambda \sin(\theta/2)$, where λ is X-ray wavelength and θ is scattering angle). The scattering intensity after subtraction of the empty cell and background was circularly averaged.

MALDI-TOF data were collected with an Ettan instrument from GE Healthcare operated in reflectron mode with the accelerating voltage held constant at 20 kV. The calibration standards used were proteins of molecular weight 1046.54 and 2464.91. The matrix used for the samples was DCTB (*trans*-2-[3-(4-*tert*-butylphenyl)-2-methyl-2-propenylidene]-malononitrile), whereas that used for calibrants was sinapinic acid.

Results and Discussion

As illustrated in Scheme 1, the basic concept of our thermal processing strategy in this case is to explore the viability of a thermally activated coalescence of the $Cu_n(SR)_m$ nanocluster seeds accompanied by interfacial C−S cleavage reactivity toward the formation of Cu_2S nanocrystals. The synthesis of thiolate-capped Cu nanoparticles as seeds or precursors was accomplished by two-phase reduction of $CuBr_4^-$ in the presence of alkanethiols. The thiolate-capped Cu nanoparticle seeds were then thermally activated to induce the C−S cleavage at the interface and the interseed coalescence forming copper sulfide nanocrystals. Note that this type of thermally induced reactivity does not occur for copper nanoparticles capped with oleic acid and oleyl amine synthesized either using separate reducing and capping agents (e.g., 1,2-hexadecanediol, oleyl amine and oleic acid), or a single reducing/capping agent (e.g., oleyl amine)[9] because of the absence of thiolates. The thermally activated interfacial reactivity and the interparticle coalescence impart the conversion of $Cu_n(SR)_m$ nanoclusters to Cu_2S nanocrystals, which is evidenced by the structural and morphological characterizations of the nanoclusters and nanocrystals.

1. Morphological Characterization. The as-synthesized Cu nanoparticles appear a light-brown color in the solution. After the thermal processing at 132 °C for a controlled period of time, the particles in the solution showed a dark brown/orange color. The particles were soluble in hexane and stable in air as supported by surface characterization, which indicates the lack of oxide formation. Figure 1A shows a TEM image for the as-synthesized decanethiolate-capped Cu nanoparticles. It is difficult to resolve the individual character of the particles because they appear to be very small (< 1 nm).

In contrast, the particles after the thermally activated processing displayed an evolution of size and shape (Figure 1B). The observation of the ordered arrays of nanoparticles with a bar-like feature (10−30 nm long and ∼5 nm wide), in sharp contrast to the as-synthesized nanoparticle precursor, indicates an effective evolution in size and shape of the nanoparticles. The presence of ordered domains of the nanoparticles and the range of the interparticle distance appear to be consistent with the presence of the decanethiolate monolayer on the nanoparticles.

Figure 2A shows another set of TEM images for the as-synthesized copper nanoparticle seeds synthesized under a higher concentration of copper precursor (using method-B with 14x excess of $CuCl_2$ and 10x excess of KBr). In this case, the nanoparticles appear to be resolved slightly better, showing an average of 0.33 (±0.03) nm in size. By further increasing the concentration of the particles in the

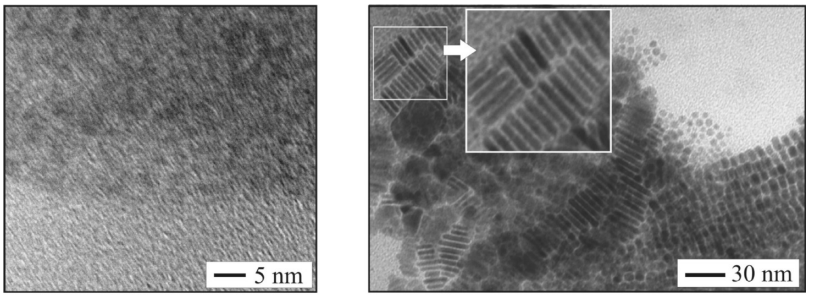

Figure 1. TEM micrographs for (A) as-synthesized DT-capped Cu nanoparticles and (B) Cu_2S nanoparticles thermally processed at 132 °C for 2 h.

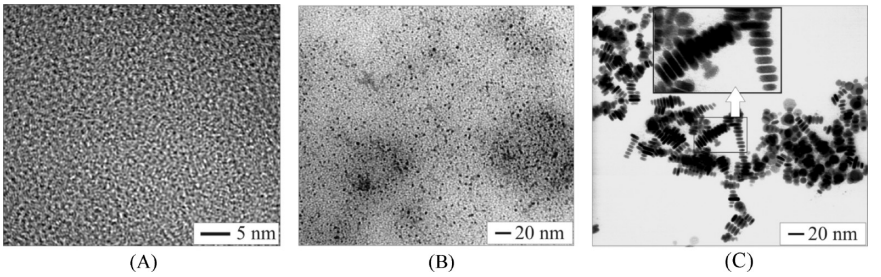

Figure 2. TEM micrographs of DT-capped Cu and Cu_2S nanoparticles synthesized using method B: (A) as-synthesized copper nanoparticles, (B) as-synthesized copper nanoparticles (a concentrated (~10×) sample of the same particles), and (C) Cu_2S nanoparticles thermally processed at 140 °C for 20 h.

sample when casting the sample solution onto the TEM-grid (~10×), slightly larger-sized particles (2.2 ± 0.4 nm, Figure 2B) were observed, which likely reflects clustering or aggregation of the particles on the carbon film. Again, after thermal processing of the particles at 140 °C for 2 h (Figure 2C), the resulting particles showed larger sizes (~10 nm) with bar-like or disklike shapes, and the particle-stacking feature similar to those in Figure 1B.

To understand first the ultrafine size feature of the as-synthesized copper nanoparticles, we analyzed a highly concentrated suspension using combined SAXS and WAXS techniques. Figure 3 shows a representative set of the combined SAXS and WAXS patterns. A peak was observed, and the peak maximum (q = 13.4 nm^{-1}) was used to calculate the interparticle distance ($d = 2\pi/q$, where d is the interparticle core distance).[33] It is interesting to find that the calculated intercore distance (0.5 nm) is smaller than the length of a decanethiol molecule (~1 nm[34]). This finding indicates that the particles are likely interdigitated via the alkyl chains to form an aggregate. The aggregation led to the reduction of the interparticle distance (inset B). Thus, the average particle size is estimated to be close to or less than 0.5 nm.

There are several additional measurements supporting the ultrafine character of the as-synthesized copper nanoparticles. One measurement involved TLC separation of the ultrafine Cu clusters (see the Supporting Information) from the solution. The separated product was first analyzed using DCP-AES technique, which confirmed the presence of copper species. The product

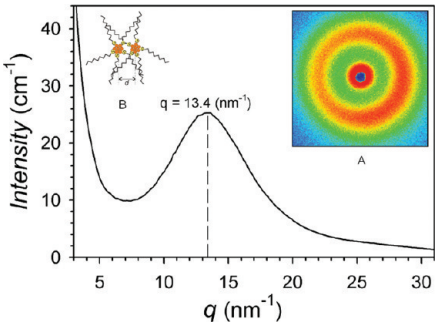

Figure 3. Combined SAXS and WAXS spectrum of the as-synthesized copper nanoparticles capped with a DT monolayer. Peak maximum: 13.4 (nm^{-1}). Error for intensity: <0.1%. Inset A: Two-dimensional WAXS scattering patterns (radial averaging). Inset B: A scheme illustrating the interparticle clustering in the concentrated suspension and the resulting interparticle distance (d).

was then analyzed using MALDI-TOF technique to determine the atomic makeup of the nanoparticles.[43] Both electrospray ionization[42,43] and MALDI-TOF[44] have been employed for such characterization because of their ability to determine nanoparticle masses without a high degree of fragmentation. In contrast to electrospray ionization where the particle requires a capping shell with ionic charge such as glutathione,[42] MALDI-TOF analysis employs a matrix that can impart a charge to the molecule or a nanoparticle with neutral capping molecules such as thiols[44] without fragmenting it. For our as-synthesized decanethiolate-capped Cu nanoparticles, peaks in the region of 600−1200 (m/z) were detected (see the Supporting Information). Although a detailed analysis is needed to pin down the corresponding structures, preliminary analysis of the peak positions for the significant peaks, along with calculated masses for the associated clusters, seemed to suggest the presence of

(33) Maye, M. M.; Lim, I-I. S.; Luo, J.; Rab, Z.; Rabinovich, D.; Liu, T.; Zhong, C. J. *J. Am. Chem. Soc.* **2005**, *127*, 1519.
(34) Han, L.; Luo, J.; Kariuki, N. N.; Maye, M. M.; Jones, V. W.; Zhong, C. J. *Chem. Mater.* **2003**, *15*, 29.

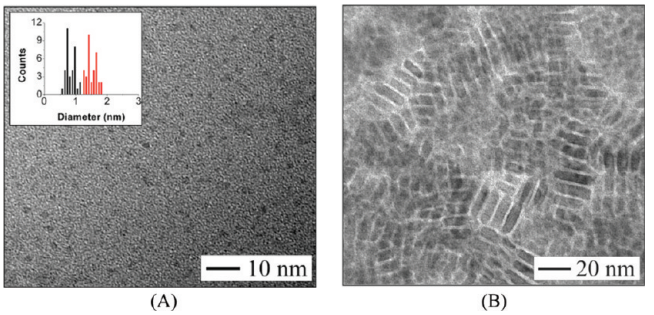

Figure 4. HR-TEM micrographs of as-synthesized DT-capped Cu_2S nanoparticles synthesized: close examination of the DT-capped Cu nanoparticles formed via thermally controlled evolution at 132 °C for (A) 1 and (B) 2 (Note that the DT used in the synthesis was 50% of that in Figure 1B). Inset: Size distributions in which the red and black bars correspond to the apparent larger and smaller particles in image A, respectively.

Cu_{5-7} clusters such as $Cu_5(SR)_4$, $Cu_5(SR)_5$, $Cu_6(SH)_3SR$, $Cu_7(SH)_4SR$, and $Cu_7(SH)_2(SR)_2$.

Insights into the size and shape evolution of the thermally processed nanoparticles were further revealed by a close examination of the morphology using HR-TEM (Figure 4). In comparison with the nanoparticles produced by 2 h processing time which showed the stacked features of larger-sized particles (Figure 4B), the shortening of the processing time was found to produce small-sized nanoparticles as evidenced by the results for 1 h thermal processing (Figure 4A). The small-sized particles showed an average size of 1.5 ± 0.2 nm. Some of the apparent dark spot features seem to be composed of 2 or 3 smaller particles with an average size of 0.9 ± 0.1 nm. These highly monodispersed particles also seem to display multiple facets.

The size and shape evolution was also found to depend on the thermal processing temperature and time. Figure 5 shows a representative set of TEM images for the nanoparticles obtained by thermal processing at 132 °C for 2 h (A) and 4 h (B). In the case of 2 h (A), the resulting nanodiscs are quite monodispersed in size, displaying an average diameter of 8.7 ± 1.1 nm and an average thickness of 4.9 ± 0.7 nm (A). The aspect ratio of the particle diameter to thickness is quite small (1.8). The tendency of self-assembly into large domains of ordering is evidenced by the observation of 1D, 2D, and 3D arrays in the assemblies.

For the nanoparticles thermally processed at 132 °C for 4 h, a further increase in size, monodispersity and aspect ratio was observed (Figure 5B). The majority of the nanoparticles display an average diameter of 10.7 ± 1.4 nm with an average thickness of 5.5 ± 0.5 nm (aspect ratio ~ 2.0), which are slightly larger than those obtained for thermal treatment at 132 °C for 2 h. In addition, a certain percentage of the particles were found to display much larger size features, with an average diameter of 31.2 ± 4.3 nm and an average thickness of 3.9 ± 0.4 nm (aspect ratio ~7). The high monodispersity is supported by the narrow size distributions, which apparently favors a great tendency of self-assembly forming large domains of 1D ordered array. The interparticle spacing in the ordered assembly is also found to be quite

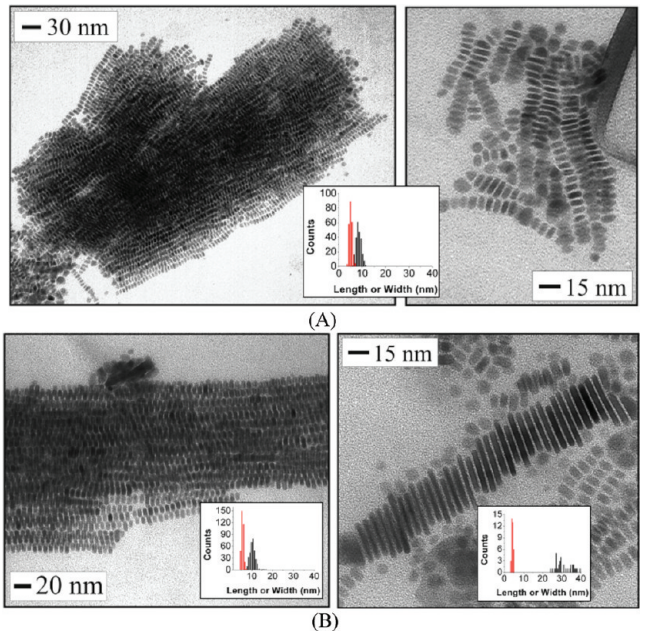

Figure 5. TEM micrographs for DT-capped Cu_2S nanoparticles obtained after thermal processing at 132 °C for (A) 2 and (B) 4 h (in each case, two sample areas were shown with different magnifications). Insets: Size distributions (black bars for disk diameter (or feature length in the image), and red bars for disk thickness (or feature width in the image)).

uniform. The particles exhibit an average interparticle edge-to-edge distance of 0.9 ± 0.2 nm, close to that expected for the interdigitation of the capping DTs on the nanoparticles.[35] The longer duration of thermal treatment seemed to increase the ordering of the particles in comparison with those obtained with a shorter duration of thermal treatment. Experiments also showed that the nanoparticles produced at other different thermal-processing temperatures or reaction times exhibited poor size monodispersity. For example, the nanoparticles obtained by thermal processing at 127 °C for 2 and 4 h were less-monodispersed and less-ordered than those obtained at 132 °C. A higher temperature (142 °C) eventually resulted in interparticle aggregation, likely due to extensive surface melting of the particles. The results suggest that the temperature between 127 and 132 °C favors the formation of highly monodispersed particles.

As shown by the data below, these thermally processed larger-sized nanoparticles are characterized by the shape of nanodiscs, which have the propensity of forming the face-to-face stacking domains. By thermal processing of copper nanoparticles (prepared using an increased amount of Br^-) at 132 °C for 4 h (A, B) and 20 h (C, D) (Figure 6), the resulting particles were found to display a predominately nanodisc shape, as reflected by assembly domains with different alignments of the nanodiscs. The hexagonal nanodiscs (7.5 ± 0.4 nm) in some domains appear to be assembled with different orientations (A). Some smaller particles (6.5 ± 0.5 nm) can also be observed around the periphery of the domains of the assembled particles (A). The formation of 1D and 2D

(35) Maye, M. M.; Luo, J.; Han, L.; Kariuki, N. N.; Zhong, C. J. *Gold Bull.* **2003**, *35*, 75.

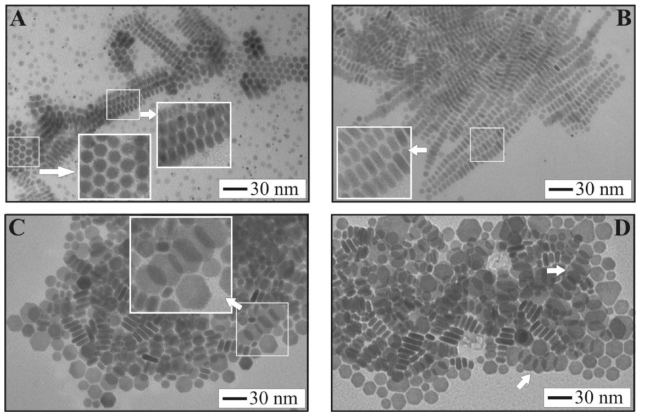

Figure 6. TEM images of DT-capped Cu_2S nanoparticles that were prepared using an increased amount of Br^-, and thermally treated for (A, B) 4 and (C, D) 20 h, both at 132 °C. Arrows indicate some example areas of ordered arrays of nanodiscs.

arrayed assemblies is evident (A, B). For the nanoparticles obtained by thermal processing for 20 h (C, D), the increase in nanodisc size is evident, ranging from about 13 to 23 nm. The hexagonal nanodiscs exhibit largely flat orientations with some particles lying on edge forming ordered domains. As indicated by the magnified views of the indicated areas in the TEM images (Figure 6), the observation of these ordered domains illustrates that these nanodiscs adopted different orientations or alignments upon self-assembly on the carbon film surface.

HR-TEM analysis provided detailed structures of the nanodiscs. Figure 7 shows a set of HR-TEM images for a sample of nanodiscs. The atomic lattices can be observed from the disk-edge (A) or the disk-face (B) directions. A measurement of the spacing of the lattice lines from the disk-edge (A) revealed a lattice of 0.198 nm. This value is in close agreement for the lattice spacing of 0.20 nm for the (110) crystal plane reported for Cu_2S nanodiscs synthesized using other methods.[6] From the lattice feature of the disk-face (B), a value of 0.188 nm is determined, which apparently also corresponds to the lattice for (110) crystal plane.[3,6] Note that lattice constants of 0.334 and 0.194 nm were reported for (002) and (110) planes, respectively, in the study of Cu_2S nanodisks obtained by other methods.[2] Because the lattice fringes of these nanodiscs are very similar to those reported for the nanodiscs synthesized by other methods.[2,3,6] Our copper sulfide nanodiscs are believed to be crystal structures identical to those derived by the other synthetic methods.[2,3,6] This finding demonstrates that our thermally activated processing approach is highly effective in converting copper nanoparticle seeds into copper sulfide nanocrystals.

The size and shape evolution of the copper nanoparticles from the thermal processing under the above conditions was also dependent on the nature of the capping monolayers. For example, the thermal processing of the as-synthesized copper nanoparticles capped with OAM/OAC monolayers[9] for 2 h at 142 °C did not reveal an observable size or shape evolution (see the Supporting Information). The copper nanoparticles are predominately ~50 nm in diameter, with a small portion of

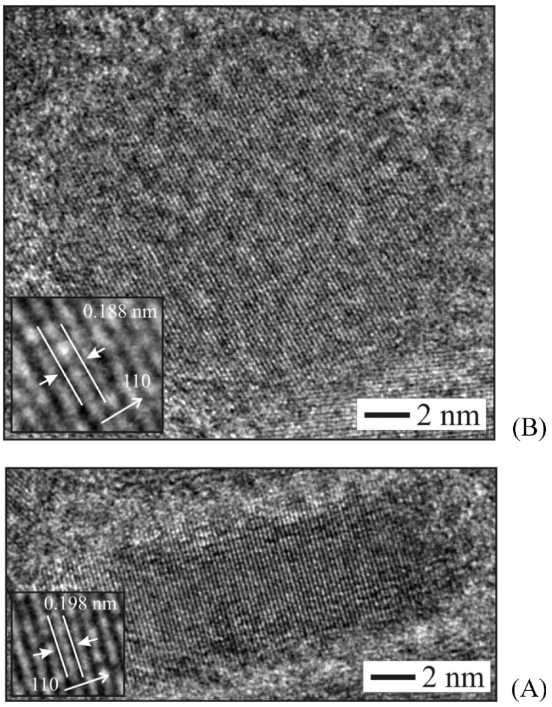

Figure 7. HR-TEM images for a single Cu_2S nanodisc: single nanodisc with an (A) edge-down and (B) face-down orientation (insets: lattice fringes that can be indexed as (110) planes).

particles less than 25 nm. The size and morphology of the nanoparticles seemed to remain unchanged after the thermal processing of the OAM/OAC-capped Cu nanoparticles.

2. Structural Characterization. XRD, XPS, and AES techniques served as diagnostic tools to determine the structural and chemical nature of the copper species and the capping monolayers of the nanoparticles.

XRD. In contrast to the fact that the copper nanoparticle seeds were too small to be detected by XRD, the copper sulfide nanocrystals displayed well-resolved XRD patterns. Figure 8a shows a typical XRD pattern for a sample of the Cu_2S nanodiscs produced by the thermal processing. The 2θ values of the peaks observed are 38.01 for (102), 46.94 for (110), 49.00 for (103), and 55.35 for (200). These peaks indexed for (102), (110), (103), and (200) planes of symmetry are characteristic of the crystallinity of Cu_2S, which are consistent with the reports for Cu_2S nanoparticles prepared by other methods.[2,3,6] In the $2\theta < 35°$ region, there appear to be additional peaks but they are not well-defined due to the high noise level. These peaks possibly originate form other nanostructures or phases of copper sulfides. As reported recently,[8c] peaks were observed in this region for Cu_2S nanorod arrays and flowers.

In comparison, the XRD pattern for a sample of the particles after the thermal processing of amine-capped Cu nanoparticle seeds showed peaks at 36.72 for (111), 42.57 for (200), 61.97 for (220), and 74.00 for (311) (Figure 8B). These peaks are characteristic of the monometallic copper nanoparticles.[9]

XPS and AES. XPS and AES provided detailed information on the oxidation state, the chemical composition,

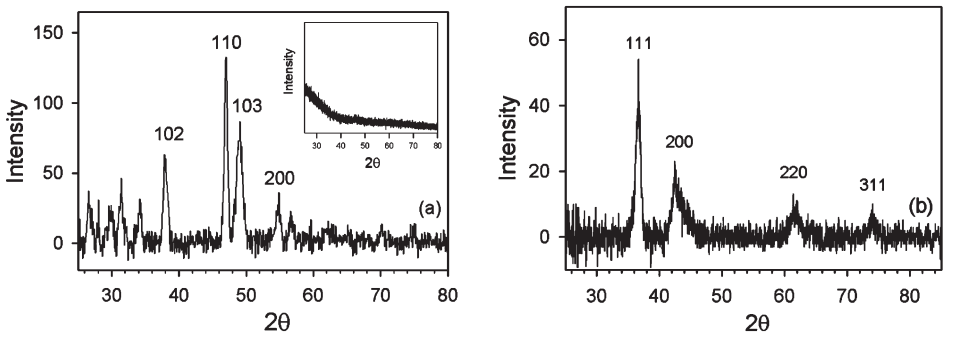

Figure 8. XRD patterns for thermally processed nanoparticles from (a) DT-capped Cu nanoparticles (inset: XRD for the precursor DT-capped Cu nanoclusters) and (b) OAM/OAC-capped Cu nanoparticles (140 °C for 2 h).

and the surface species for both the as-synthesized copper nanoparticles and the thermally processed copper sulfide nanocrystals. The binding energy for C(1s) was used as an internal reference to eliminate the charging effect.[36] Figure 9A shows a typical XPS spectrum in the Cu(2p) region for the as-synthesized copper nanoparticles. A single set of doublet peaks characteristic of Cu(2p), i.e., 932.0 eV for Cu($2p_{3/2}$) and 952.0 eV for Cu($2p_{1/2}$), is identified in the Cu(2p) region that closely matches literature values.[37,38] Because of the proximity of binding energies for Cu^0 and Cu^+, this peak could not be used to make a definitive determination of the copper oxidation state in the sample. To address this issue, LMM Auger spectroscopic measurement was performed with this sample. Figure 9B shows the LMM Auger peak of Cu for the as-synthesized copper nanoparticles. The detection of the peak at 569.2 eV indicates that the nanoparticle cores are composed of monatomic copper. The data showed no indications of oxidation or conversion of copper into other species such as Cu_2O or Cu_2S. The AES Cu(LMM) peak for Cu_2S nanodiscs was observed at 571.2 eV (dash line in Figure 9B). This peak is slightly higher than the LMM Auger peak reported for copper (568.1 eV) and for Cu_2O (570.1 eV).[39] The slightly higher binding energy could be due to the combination of a higher partial charge on copper as a result of surface binding to sulfur or thiolate species and possible surface charging effect of the sample. Nevertheless, the results confirm the zero valence (Cu(0)) for the oxidation state of the as-synthesized copper nanoparticles.

Figure 10 shows a typical set of XPS spectra in Cu(2p) (A) and S(2p) (B) regions for DT-capped Cu nanoparticles before and after the thermal processing. In Cu(2p) region (A), a single set of doublet peaks characteristic of Cu(2p), i.e., 932.7 eV for Cu($2p_{3/2}$) and 952.5 eV for Cu($2p_{1/2}$), is identified for the Cu_2s nanodiscs obtained by thermal processing (a). The peak positions are higher than peaks for the as-synthesized Cu nanoparticles (932.0 eV

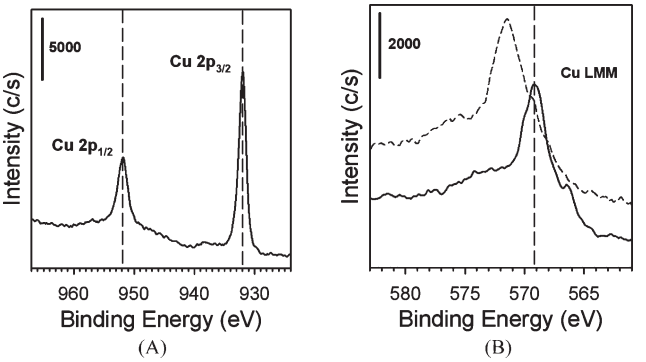

Figure 9. (A) XPS spectrum in the Cu2p region and (B) AES spectrum in the Cu LMM region for as-synthesized copper nanoparticles (the dashed curve represents the AES spectrum for Cu_2S nanoparticles).

for Cu($2p_{3/2}$) and 952.0 eV for Cu($2p_{1/2}$) (b)) by about 0.6 eV, which is in agreement with the difference of the oxidation states of copper between these two samples.

In the S(2p) region (B), the spectral deconvolution of the S(2p) bands with a Gaussian profile reveals the presence of two sets of S(2p) doublets (S($2p_{3/2}$) to the S($2p_{1/2}$)). This deconvolution into one set of doublets at the higher binding energy region (i.e., thiolates) could not fit well in the lower-binding energy envelope, suggesting the presence of sulfides. For the doublet fitting, the fitting constraints for the doublet of peaks involved a half width at full maximum (HWFM) of 1.0 ± 0.10 eV and a binding energy difference of ~1.2 eV between $2p_{3/2}$ and $2p_{1/2}$ peaks. Note that the relative atomic ratio of Cu to S was found to be about 1.8, which possibly reflected the presence of more Cu atoms than the capping S-species in the small clusters. In comparison with the thiolate peaks at 163.1 ($2p_{1/2}$) and 161.9 eV ($2p_{3/2}$) for copper nanoparticles (curve a), the thermally treated nanoparticles showed a first set of doublets at 163.1 eV ($2p_{1/2}$) and 162.1 eV ($2p_{3/2}$), and a second set at 162.1 eV ($2p_{1/2}$) and 161.1 eV ($2p_{3/2}$) (curve b). These results are consistent with the chemical identities of the two sets of doublets corresponding to thiolates and sulfides, respectively (see the Supporting Information).[40,41] There is clearly a small

(36) Wang, L.; Luo, J.; Maye, M. M.; Fan, Q.; Rendeng, Q.; Engelhard, M. H.; Wang, C.; Lin, Y.; Zhong, C. J. *J. Mater. Chem.* **2005**, *15*, 1821.
(37) Wu, C. K.; Yin, M.; O'Brien, S.; Koberstein, J. T. *Chem. Mater.* **2006**, *18*, 6054.
(38) Ma, X.; Wang, G.; Yukimura, K.; Sun, M. *Surf. Coat. Technol.* **2007**, *201*, 6712.
(39) Chavez, K. L.; Hess, D. W. *J. Electrochem. Soc.* **2001**, *148*, G640.
(40) Kariuki, N. N.; Luo, J.; Hassan, A.; Lim, I. I. S.; Wang, L.; Zhong, C. J. *Chem. Mater.* **2006**, *18*, 123.
(41) Hostetler, M. J.; Zhong, C. J.; Yen, B. K. H.; Anderegg, J.; Gross, S. M.; Evans, N. D.; Porter, M. D.; Murray, R. W. *J. Am. Chem. Soc.* **1998**, *120*, 9396.

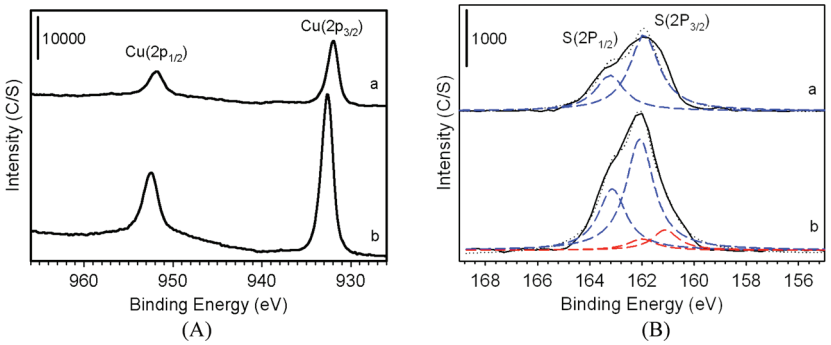

Figure 10. XPS spectra in the (A) Cu2p and (B) S2p regions for DT-capped Cu nanoparticles (a) before and (b) after thermal treatment (132 °C for 2 h). The spectral deconvolution was based on full width at half-maximum (fwhm) of ~1.05 eV for the S2p peaks; the dashed and the dash-dot curves represent deconvolution curves; the closed circles represent the experimental spectral data. The solid line represents the experimental data, and the dashed and dotted lines represent spectral deconvolution results.

fraction of the envelope in the lower-binding energy region (~161.5 eV) which was not fitted by the spectral deconvolution. This lower-binding energy fraction is very close to the S(2p) peaks detected for $Au(I)_2S$ and S_2^- adsorbed on Au substrates (see the Supporting Information), further substantiating the composition of Cu_2S in the nanocrystals. The intensity of the sulfide peak is lower than that for the thiolates because of the electron attenuation effect. The results thus confirm that the capping monolayer on the copper sulfide nanodiscs consists of decanethiolate species. An analysis of the relative intensity of Cu and S peaks showed a Cu:S ratio of 1.6 for the Cu_2S sample, which was slightly smaller than the expected ratio likely reflecting the presence of surface capping thiolates on the nanocrystals.

As a control experiment, the thermally processed Cu nanoparticles capped with oleyl amine were also examined using XPS. The doublet for Cu(2p) peaks (Figure 11A) was observed at 932.3 eV for $Cu2p_{3/2}$ and 952.2 eV for $Cu2p_{1/2}$ for the as-synthesized amine-capped Cu nanoparticles (solid curve), and at 932.7 eV for $Cu2p_{3/2}$ and 952.6 eV for $Cu2p_{1/2}$ for the thermally processed amine-capped Cu nanoparticles (dashed curve). The peaks of ~944 and ~964 eV correspond to satellite peaks. In this case, little change in the spectroscopic characteristics was observed before and after thermal processing. The oxidation state of the copper species corresponds to Cu(0). Furthermore, the detection of the N1s band (Figure 11B) confirms that the capping shell structure consists of amines for the amine-capped Cu nanoparticles.

In contrast to the formation of Cu_2S for thermal processing of DT-capped Cu nanoparticles, the amine-capped Cu nanoparticles remain largely Cu nanoparticle cores. This is also evidenced by the XRD data for the thermally processed amine-capped nanoparticles (see Figure 8), which is characteristic of Cu nanoparticles.[9]

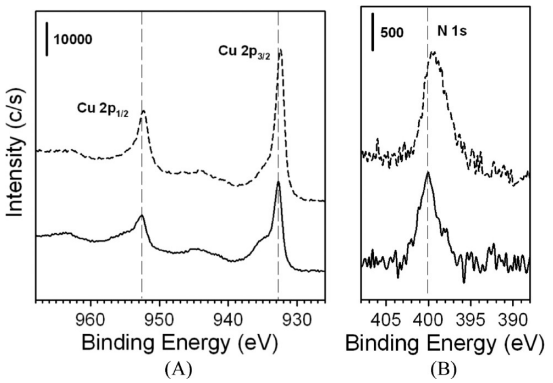

Figure 11. XPS spectra in the (A) Cu2p and (B) N1s regions. Solid curves, as-synthesized OAM- and OAC-capped Cu nanoparticles; dashed curves, thermally processed OAM/OAC-capped Cu nanoparticles in solution for 1 h.

3. Mechanistic Considerations. The formation of copper sulfide nanodiscs, as reported for the previous methods,[1−3] relied on thiol thermolysis in which the copper complexes react with the thermolyzed thiols. The surface energetic difference of different crystal facets was proposed[3] to explain the thermodynamically favored C−S cleavage of the adsorbed thiols on higher-energy surfaces over lower-energy surfaces, and the nanodisc morphology as a result of a faster growing ⟨100⟩ direction over the ⟨001⟩ direction. The thiol thermolysis provides sulfur monomer through C−S bond thermolysis (C−S bond cleavage). In this case, the shape formation relies on the face-sensitive surface reactivity. On the basis of the reaction kinetics[3] and our experimental results, a combination of two concurrent processes is believed to be operative in the formation of the copper sulfide nanodiscs, as illustrated in Scheme 1. The first involves the thermally activated C−S cleavage at the Cu−SR interface, and the second involves the interseed coalescence of the partially molten $Cu_n(SR)_m$ seeds. The latter takes advantage of the particle size effect on the melting temperature of nanoparticles,[26] whereas the former is catalyzed by the copper nanoparticle surface.[3,6] The requirement of these two elements is supported by the absence of Cu_2S nanodisc formation for copper nanoparticles capped with oleic acid and/or oleyl amine. The thermally activated

(42) Shichibu, S.; Negishi, Y.; Tsukuda, T.; Teranishi, T. *J. Am. Chem. Soc.* **2005**, *127*, 13464.
(43) Tracy, J. B.; Crowe, M. C.; Parker, J. F.; Hampe, O.; Fields-Zinna, C. A.; Dass, A.; Murray, R. W. *J. Am. Chem. Soc.* **2007**, *129*, 16209.
(44) Dass, A.; Stevenson, A.; Dubay, G. R.; Tracy, J. B.; Murray, R. W. *J. Am. Chem. Soc.* **2008**, *130*, 5940.

interfacial reactivity and the interparticle aggregative nucleation and coalescence impart the conversion of $Cu_n(SR)_m$ nanoclusters to Cu_2S nanocrystals capped with thiolates $[Cu_{2n'}(S)_{n'}](SR)_{m'}$ via

$$Cu_n(SR)_m \rightarrow Cu_n(S)_x(SR)_{m-x} \quad (1)$$

$$Cu_n(S)_x(SR)_{m-x} \rightarrow \ldots \rightarrow [Cu_{2n'}(S)_{n'}](SR)_{m'} \quad (2)$$

where n' and m' represent the number of Cu atoms and the number of thiolates in the final nanodiscs. Eq 1 involves C-S cleavage, whereas Eq 2 involves aggregative nucleation and growth.

Because the nanodisc growth involves the coalescence of small-sized $Cu_n(S)_x(SR)_{m-x}$ particles onto the larger-sized Cu_2S nanodisc $[Cu_{2n'}(S)_{n'}](SR)_{m'}$, the surface capping structure must have played an important role in the shape formation. As noted earlier, the initial shape of the seed is characterized by multifacets (e.g., a decahedron). The growth rate along crystal facets of the nanodisc, as regulated by the adsorption−desorption of surface thiolates, is dependent on a combination of three parameters, the relative binding strength of thiolates, the tendency of C−S cleavage, and the interparticle coalescence in terms of surface free energy. In this case, the first two parameters, the relative binding strength of thiolates and the tendency of C−S cleavage, are expected to operate similarly to those proposed for the synthesis of copper sulfides by the thermolysis method.[3] Kinetically, they favor a faster growth rate along the ⟨100⟩ direction of the hexagonal nanodiscs than along the ⟨001⟩ direction. The third parameter, i.e., the interparticle coalescence, is related to the cohesive adsorption energy of the thiolate monolayer on the particle surface, which partially controls the nanodisc shape evolution. Because the cohesive energy is the stabilization energy due to the chain−chain cohesive interaction, this energy is greater on a larger surface (e.g., (001) plane) than on a smaller surface (e.g., (100) plane).[26b] The interparticle coalescence requires the desorption of the monolayer from the surface and re-encapsulation after the coalescence. It can therefore kinetically slow down the growth rate along the ⟨001⟩ direction (i.e., in the direction normal to the disk platelet) in comparison with all other side directions characteristic of the ⟨100⟩ direction. Scheme 2 illustrates the relative growth rates of a nanodisc along the different facet directions under these control parameters.

In this mechanistic consideration, the combination of the thiolate adsorption/desorption, the C−S cleavage, and the interparticle coalescence determines the final size and shape of the nanodisc, a detailed correlation among these three parameters is part of our ongoing work. It is important to emphasize that this process is not a simple digestive ripening of smaller particles because it involves an aggregative growth process distinctively different from traditional ripening phenomenon and a reactive carbon−sulfur bond cleavage controlled by the catalytic effect of copper under the specified temperatures.

Scheme 2. Schematic Illustration of the Relative Rates for the Interparticle Coalescence and the Nanocrystal Growth in the Formation of a Copper Sulfide Nanodisc

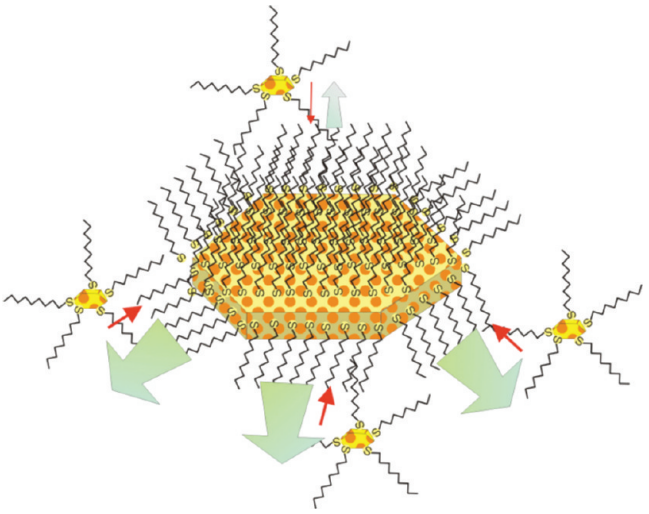

Conclusions

In conclusion, the combined weight of the results from the different characterizations has demonstrated that copper sulfide nanodiscs with controllable sizes and shapes can be fabricated by thermally activated processing of ultrafine (~0.5 nm) copper nanoparticles encapsulated with thiolates ($Cu_n(SR)_m$). These nanodiscs are stable and display remarkable ordering upon self-assembly. The thermally activated coalescence of the nanocluster seeds is accompanied by an interfacial C−S bond cleavage toward the formation of Cu_2S nanocrystals. The shape formation is believed to be determined by the difference of the growth rates along crystal facets of the nanodisc, which are regulated by the differences in the adsorption−desorption of surface thiolates, the C−S cleavage activity, and the interparticle coalescence. There are several significant findings that enable the success of this novel approach. The first is the ability to create the ultrafine copper nanoclusters, which to the best of our knowledge is not demonstrated in previous reports. Second, the small nanoclusters are demonstrated to undergo a thermally activated coalescence that is accompanied by a concurrent C−S bond cleavage toward the formation of a copper sulfide nanodisc, which is not known in existing approaches to synthesizing copper sulfide nanodiscs. Our approach can potentially fine-tune the size and shape of the Cu_2S nanocrystals by controlling the relative binding strength of thiolates, the C−S cleavage reactivity, and the interparticle coalescence activity. An in-depth investigation focuses on understanding how the temperature threshold among the cleavage, coalescence, and aggregation depends on the size and monodispersity of the original Cu nanoclusters. The copper nanoclusters and copper sulfide nanodiscs are stable in air, which is critical for the exploitation of the electrical conductivity and catalytic and photochemical properties of the nanomaterials. Preliminary testing of the Cu_2S nanoparticles assembled as thin films on electrode surfaces as

chemiresistor sensing materials and as photoelectrochemical materials showed interesting responses to the sorption of small gas/vapor molecules, and to on/off switching of UV light, which are subjects of our ongoing investigations. The coupling of thermally activated coalescence and interfacial bond cleavage of ultrafine nanoclusters toward the formation of size-, shape-, and composition-controllable nanocrystals could find applications in nanoengineering a variety of semiconducting nanocrystals, which have potential applications in nanostructured electronic, sensing, and photochemical devices.

Acknowledgment. This research work was supported by AFRL/RHPG (FA8650-07-2-6836) and in part by the National Science Foundation (CHE 0848701, and CHE 0349040). XPS and part of the TEM measurements were performed in EMSL, a national scientific user facility sponsored by the DOE's Office of Biological and Environmental Research at PNNL.

Supporting Information Available: Additional data of XPS, TEM, and MALDI-TOF (PDF). This material is available free of charge via the Internet at http://pubs.acs.org/.